electronics

MDPI

Article

Physical Layer Security in RIS-NOMA-Assisted IoV Systems with Uncertain RIS Deployment

Jinyuan Gu [1], Zhao Zhang [2], Wei Duan [2], Feifei Song [1] and Huaiping Zhang [1,*]

[1] Kangda College of Nanjing Medical University, Lianyungang 222000, China; gujinyuan@njmu.edu.cn (J.G.); feifei_song@njmu.edu.cn (F.S.)
[2] School of Information Science and Technology, Nantong University, Nantong 226019, China; 2110310026@stmail.ntu.edu.cn (Z.Z); sinder@ntu.edu.cn (W.D)
* Correspondence: zhhp@njmu.edu.cn

Abstract: Reconfigurable intelligent surfaces (RISs), as an emerging radio technology, are widely used to expand the transmission distance and structure cascade channels to improve the performance of communication systems. However, based on the continuous development of wireless communication technology, as Internet of Vehicles (IoV) communication systems assisted with RIS and non-orthogonal multiple access (NOMA) can improve the overall transmission rate and system performance, the physical layer security (PLS) issue has gradually attracted attention and has become more and more important in the application of the system. In this paper, our aim is to investigate the potential threats for PLS, where an RIS is utilized in order to improve the security of wireless communications. In particular, we consider the non-fixed RIS location and wiretapping behavior of eavesdroppers on the data in this work, and further analyze the maximum safe-rate for above location assumptions. Numerical results reveal that RIS provides significant advantages on security performance, as well as providing a useful reference for the security design of future wireless communication systems, which verify the correctness of our analysis and the effectiveness of the proposed scheme.

Keywords: non-orthogonal multiple access (NOMA); reconfigurable intelligent surfaces (RIS); Internet of Vehicles (IoV); physical layer security (PLS); safe-rate

Citation: Gu, J.; Zhang, Z.; Duan, W.; Song, F.; Zhang, H. Physical Layer Security in RIS-NOMA-Assisted IoV Systems with Uncertain RIS Deployment. *Electronics* **2024**, *13*, 4437. https://doi.org/10.3390/electronics13224437

Academic Editor: Aryya Gangopadhyay

Received: 17 October 2024
Revised: 9 November 2024
Accepted: 11 November 2024
Published: 12 November 2024

1. Introduction

With the development of vehicle networking systems, wireless transmission coverage, high energy efficiency and secure communication have become the primary tasks of evaluating vehicle networking communication systems [1,2]. For the Internet of Vehicles (IoV), they can share information not only with infrastructure (e.g., roadside units (RSUs) through vehicle-to-infrastructure (V2I) communication), but also with vehicles through vehicle-to-vehicle (V2V) communication [3]. In addition, automatic driving, intelligent driving-assist systems, traffic flow and urban traffic management also bring exponential growth of massive data and computing resources consumption. Critical and real-time collaborative control messages require strict delay restrictions, while the transmission of multimedia entertainment application information can accommodate a certain degree of delay, which poses a great challenge for managing the interaction of vital information, task unloading and realizing large-scale model (LSM)-based decision-making across many heterogeneous nodes within the framework of the Internet of Vehicles [4]. The wide applications of the IoV based on artificial intelligence (AI) have aroused significant concern about the IoV, which involves heterogeneous computing-intensive and delay-intolerant tasks. The on-board resources of consumer vehicles cannot meet such requirements, so researchers introduced the technology of multiple-access edge computing (MEC), which can expand the computing power of vehicle networks by allowing vehicles to offload some tasks to MEC servers. The authors in [5] minimize energy consumption, and develop a method based on deep reinforcement learning (DRL) to offload tasks to roadside units (RSUs) or

other vehicles. Similarly, the authors in [6,7] use the method based on DRL to unload tasks. In addition, the coverage of wireless communication networks based on high-cost base stations (BSs) is still limited, and it is impossible to provide continuous, reliable and high-throughput basic services [8,9]. Therefore, there are obvious technical obstacles to realize reliable and extensible wireless transmission in the IoV, which imposes great restrictions on the deployment of the above-mentioned intelligent vehicles and transportation systems.

As a novel wireless communication technology, RISs can utilize a series of reflective elements to modulate electromagnetic wave signals and transmit them to the receiver; thus, they can effectively assist the communication between the transmitter and the receiver. For example, when the user is in an environment with poor communication quality, the RIS deployed in the surrounding area can reflect the signal to the required position to assist communication. Compared with the traditional antenna and base station technology, RISs have higher spectral efficiency, lower power consumption and better privacy [10,11]. In order to ensure low latency, the IoV needs ubiquitous ultra-reliable, low-latency and high-speed wireless communication. In this respect, RIS-assisted communication is a revolutionary way to improve the quality of wireless communication by adjusting the wireless propagation path [12]. RISs can reconstruct the wireless channel by using electromagnetic elements to manipulate incident waves, thus enhancing the system throughput and improving the quality of service (QoS) of edge users [13,14]. Although BSs are the central hub of information exchange, they may not be able to achieve full coverage in urban application scenarios. Some RISs are deployed in a fixed configuration, while others are flexibly and adaptively configured by drones to adapt to the complexity of wireless channels [15–17]. On the basis of this framework, all vehicles in the IoV as terminal nodes can not only effectively transmit key information, but also offload local computing tasks to the edge or cloud server for processing. However, the hybrid architecture integrating RISs and BSs requires advanced hybrid beamforming, including digital beamforming at BSs and analog beamforming at passive RISs, thus maximizing system throughput and reducing mutual interference. In addition, the combination of RISs and non-orthogonal multiple access (NOMA) can further improve the performance of these systems.

1.1. Related Work

In recent years, the rational use of secure channel capacity has become a focus of discussion among researchers and scholars [18,19], where the secrecy capacity of the transmitted data is investigated and the system is able to reach the maximum transmission rate between a legitimate transmitter and receiver, but this scheme is subject to the limitations of the information available to unauthorized receivers. The authors of [18] proved that for discrete memoryless channels, the perfect secrecy capability is actually the difference in capacity between two users and generalized similar results to Gaussian channels [20]. A study considered the case of full channel state information (CSI), where the transmitter has access to the channel gains of both the legitimate receiver and the eavesdropper, and this secrecy capacity under the full CSI assumption was used as an upper bound on the secrecy capacity when only the CSI of the legitimate receiver is known on the transmitter. The authors of [21] also proposed a low-complexity on or off power allocation scheme that achieves near-optimal performance using only the primary channel CSI. More specifically, the scheme is shown to be asymptotically optimal when the average signal-to-noise ratio (SNR) reaches infinity, achieving the secrecy capability assumed by full CSI. All the above studies show that channel fading has a positive effect on the secrecy capability and rate adaptation based on channel CSI. Therefore, PLS as a technology based on the physical characteristics of the communication channel to protect the security of the communication system has gradually become an important research direction in the field of information security. PLS techniques utilize the physical characteristics of the communication channel, such as signal attenuation, multipath propagation, and time-varying properties, to design security mechanisms that enhance the security of the communication system during the transmission of data [22]. Researchers are committed to continuously improving the per-

formance and reliability of PLS techniques to cope with increasingly complex and diverse security threats. In [23], the authors utilized RIS to tackle threats faced by vehicles (e.g., leaked data, hack attack, and jammer). The authors also proved that the security of IoV systems could be ensured with enough RIS elements. In [24], the PLS for RIS-aided vehicle-to-vehicle (V2V) wireless systems was investigated and two eavesdropping models were introduced. It was demonstrated that the optimizations of the RIS location and elements number could significantly improve the security of IoV environments, as well as actively deal with the challenges of eavesdroppers. And the features of PLS can effectively deal with some of the challenges faced by traditional cryptography, such as key management and side-channel attacks, as well as provide additional security guarantees. Currently, the commonly used PLS schemes are non-orthogonal multiple access (NOMA) [25], artificial noise (AN), and cooperative jamming [26].

Since eavesdroppers are unable to decode the information correctly after eavesdropping the data, researchers often employ artificial noise generation at the transmitter to reduce the quality of the received data for eavesdroppers [27,28] and to improve the security and reliability of the communication system. For some application scenarios, real-time generation, injection and processing of artificial noise signals are required, which need to be supported by corresponding hardware resources, increasing the system cost and energy consumption, in order to avoid excessive introduction of noise leading to degradation of communication quality or insufficient security enhancement. Recently, NOMA has been considered as a promising technology, which can improve the spectrum and energy efficiency [29]. The advantage of NOMA is that it can accommodate more users on the same resource block, use superposition coding at the sending terminal and continuous interference cancellation at the receiving terminal [30], which can reduce the interference of users with better channel quality to users with weaker channel quality, thus improving user fairness and reducing the probability of channel blockage in the IoV. Based on various channel conditions required by NOMA, RIS can be used for the intelligent control of random channels, which has been further discussed in recent research. However, most of these works do not consider in detail the influence of the number of RIS components on the safe-rate of data transmission under the NOMA principle.

1.2. Motivations and Contributions

In the RIS-NOMA-assisted IoV communication system, the secrecy capability can be significantly improved even in the presence of eavesdroppers. RIS can help to suppress the interference of communication signals by malicious eavesdroppers by adjusting the characteristics of the reflected signals, thus improving the security of the system [31]. RIS is also able to optimize the transmission path of the signals to reduce the signal leakage and the possibility of eavesdropping, as well as enhance the security of the channel links. In previous studies, the location of RIS is often fixed and unchanged, and how location change of the RIS can not only affect the quality of data transmission to users, but also further affect the overall safe-rate and performance of data transmission in the presence of eavesdroppers is not considered. For this reason, it is necessary to explore the impact of RIS location changes on the overall security rate of the system so as to maximize the security rate of data transmission for legitimate users.

- We propose an RIS-NOMA system consisting of a remote user, a near user and an eavesdropper, in which the eavesdropper wiretaps on the data transmission over the wireless channel. The maximum security rate under different RIS positions is analyzed and derived.
- The balance between the RIS deployment location and the channel security rate is investigated, and a trade-off between between the locations of far and near users is also considered.
- Numerical results verify the correctness of our analysis as well as the effectiveness of the proposed scheme, which provides a significant improvement in terms of the safe-rate.

2. System Model and Proposed Scheme

This work considers an RIS and NOMA-assisted secure communication system, as shown in Figure 1, which consists of the transmitting source (S), the RIS, two legitimate users D_1 and D_2, and an eavesdropper E. For the channel model, we assume that all nodes are equipped with single antenna, considering that S and D_1, D_2 are known to the eavesdropper to wiretap on the desired data X within a long distance. With $X = x_1 + x_2$, the valid data received by D_1 are x_1, and the valid data received by D_2 are x_2. Clearly, since the data received by D_1 and D_2 are both on the broadcasting channel, the safe-rate is extremely low. As the element size of RIS is much smaller than the RF signal wavelength, the elements are able to reflect the incident signal to each direction with constant gain. Furthermore, each element of the RIS is intelligently controllable, and the reflecting elements can control the phase shift.

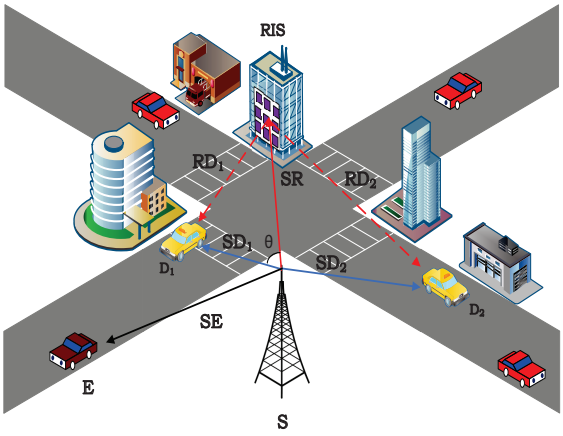

Figure 1. RIS-NOMA-assisted wireless network security communication system model.

As shown in Figure 1, the direct channels from S to RIS, user D_1, user D_2 and eavesdropper E are, respectively, expressed as $h_i, i = \{SR, SD_1, SD_2, SE\}$; the reflection channel of RIS is $h_j, j = \{RD_1, RD_2\}$. In the model, user D_2 is considered to be further away from the transmitter than user D_1; thus, the channel gain of $h_{SD_2}(H_2)$ is considered to be less than $h_{SD_1}(H_1)$. $\|\cdot\|$ represents the norm of the vector. The angle of the RIS deployment position relative to the emission source is θ in [0,180]. Because the NOMA scheme will actively consider the fairness of users, there will be differences in setting the power distribution coefficients. The power distribution factors of service user D_1 and user D_2 are a_1 and a_2, $a_1 + a_2 = 1$, and the transmission data at S is $X = a_1x_1 + a_2x_2$, where x_1 and x_2 are the expected signals of D_1 and D_2, respectively.

2.1. Power Allocation Discussion

2.1.1. Power Allocation Strategy with $a_1 < a_2$

In this section, to ensure fairness among users, we discuss power allocation for two different situations. When $a_1 < a_2$, the RIS is equipped with n fixed elements to serve different users with the same number of elements. The channel gains from the transmitter S to the RIS and from the RIS to user D_1 are $\mathbf{h}_{SR} \in \mathbb{C}^{N\times 1}, \mathbf{h}_{RD_1} \in \mathbb{C}^{N\times 1}$. Similarly, the channel gains from S to RIS and RIS to D_2 can be expressed as $\mathbf{h}_{SR} \in \mathbb{C}^{N\times 1}, \mathbf{h}_{RD_2} \in \mathbb{C}^{N\times 1}$. In addition, it is assumed that all channels experience Rayleigh fading distribution, and the signals received by users D_1 and D_2 can be expressed as

$$y_{D_1} = (\sqrt{a_1 P}x_1 + \sqrt{a_2 P}x_2)(h_{SD_1} + \mathbf{h}_{RD_1}^H \mathbf{\Theta}_1 \mathbf{h}_{SR}) + n_{D_1}, \quad (1)$$

$$y_{D_2} = (\sqrt{a_1 P}x_1 + \sqrt{a_2 P}x_2)(h_{SD_2} + \mathbf{h}_{RD_2}^H \mathbf{\Theta}_2 \mathbf{h}_{SR}) + n_{D_2}, \quad (2)$$

where P is the transmission power at S, x_1 and x_2 are the transmitted data, $\mathbb{E}[|x|^2] = 1$, and the phase shift matrix of RIS at user D_1 is $\mathbf{\Theta}_1 = \alpha diag(e^{j\phi_1}, \ldots, e^{j\phi_N})$. The phase shift matrix at user D_2 is $\mathbf{\Theta}_2 = \alpha diag(e^{j\psi_1}, \ldots, e^{j\psi_N})$, $\alpha \in (0, 1]$ is the amplitude reflection coefficient. The additive white Gaussian noise (AWGN) at both D_1 and D_2 is characterized by a mean value of zero and a variance of σ^2.

In the communication system assisted by RIS-NOMA, according to the decoding principle of NOMA, user D_1 will first decode x_2 with x_1 as interference. After successfully decoding x_2, user D_2 decodes x_1 through SIC. Therefore, the SNRs of user D_1 and user D_2 can be, respectively, given as

$$\gamma_{D_1,x_2} = \frac{a_2 P|h_{SD_1} + \mathbf{h}_{RD_1}^H \mathbf{\Theta}_1 \mathbf{h}_{\mathrm{SR}}|^2}{a_1 P|h_{SD_1} + \mathbf{h}_{RD_1}^H \mathbf{\Theta}_1 \mathbf{h}_{\mathrm{SR}}|^2 + \sigma^2}, \tag{3}$$

$$\gamma_{D_1,x_1} = \frac{a_1 P|h_{SD_1} + \mathbf{h}_{RD_1}^H \mathbf{\Theta}_1 \mathbf{h}_{\mathrm{SR}}|^2}{\sigma^2}, \tag{4}$$

$$\gamma_{D_2,x_2} = \frac{a_2 P|h_{SD_2} + \mathbf{h}_{RD_2}^H \mathbf{\Theta}_2 \mathbf{h}_{\mathrm{SR}}|^2}{a_1 P|h_{SD_2} + \mathbf{h}_{RD_2}^H \mathbf{\Theta}_2 \mathbf{h}_{\mathrm{SR}}|^2 + \sigma^2}. \tag{5}$$

Similarly, the SNR of eavesdropper is $\gamma_{E,x_1} = \frac{a_1 P|h_{SE}|^2}{\sigma^2}$, $\gamma_{E,x_2} = \frac{a_2 P|h_{SE}|^2}{a_1 P|h_{SE}|^2 + \sigma^2}$. Therefore, the achievable rates for the received data x_1 and data x_2 are, respectively, expressed as

$$R_{x_1} = \mathbb{E}\{\log_2(1 + \gamma_{D_1,x_1})\}, \tag{6}$$

$$R_{x_2} = \mathbb{E}\{\log_2[1 + min(\gamma_{D_1,x_2}, \gamma_{D_2,x_2})]\}, \tag{7}$$

where $\mathbb{E}[x]$ is the expected value of x; the eavesdropping rates on data x_1 and data x_2 by the eavesdropper are as follows:

$$R_{\mathrm{E}x_1} = \mathbb{E}\{\log_2[1 + \gamma_{Ex_1}]\}, \tag{8}$$

$$R_{\mathrm{E}x_2} = \mathbb{E}\{\log_2[1 + \gamma_{Ex_2}]\}. \tag{9}$$

Finally, the secrecy rate of data x_1 and data x_2 can be further obtained as

$$\begin{aligned} R_{Sx_1} =& R_{x_1} - R_{Ex_1} \\ =& [\log_2(1 + \gamma_{D_1,x_1}) - \log_2(1 + \gamma_{Ex_1})]^+, \end{aligned} \tag{10}$$

$$\begin{aligned} R_{Sx_2} =& R_{x_2} - R_{Ex_2} \\ =& [\log_2(1 + min(\gamma_{D_1,x_2}, \gamma_{D_2,x_2})) \\ & - \log_2(1 + \gamma_{Ex_2})]^+, \end{aligned} \tag{11}$$

where $[x]^+ = max(0, x)$. Then, the secrecy sum-rate of the data can be obtained

$$R_S = R_{Sx_1} + R_{Sx_2}. \tag{12}$$

In the communication system with NOMA, in order to ensure fairness, a larger power allocation factor will be assigned to the poor channel, and $a_1 + a_2 = 1$. When $a_1 < a_2$, the user D_1 is closer to the transmitting source, and when $a_1 < a_2$, the channel gain can be expressed as $\mathbf{h}_{SD_1} > \mathbf{h}_{SD_2}, \mathbf{h}_{RD_1} > \mathbf{h}_{RD_2}$. Therefore, it can be further deduced from Equations (3)–(5) as $\gamma_{D_1,x_2} > \gamma_{D_2,x_2}$, $min(\gamma_{D_1,x_2}, \gamma_{D_2,x_2}) = \gamma_{D_2,x_2}$, so Equation (11) can be rewritten as follows:

$$R_{Sx_1} = [\log_2(1 + \gamma_{D_1,x_1}) - \log_2(1 + \gamma_{Ex_1})]^+, \tag{13}$$

$$R_{Sx_2} = [\log_2(1 + \gamma_{D_2,x_2}) - \log_2(1 + \gamma_{Ex_2})]^+. \tag{14}$$

Thus, Equation (12) can be further written as

$$\begin{aligned} R_s &= \log_2\left(\frac{1+\gamma_{D_1,x_1}}{1+\gamma_{E,x_1}}\right)+\log_2\left(\frac{1+\gamma_{D_2,x_2}}{1+\gamma_{E,x_2}}\right) \\ &= \log_2\left[\frac{\left(1+\gamma_{D_1,x_1}\right)\left(1+\gamma_{D_2,x_2}\right)}{\left(1+\gamma_{E,x_1}\right)\left(1+\gamma_{E,x_2}\right)}\right]. \end{aligned} \tag{15}$$

2.1.2. Power Allocation Strategy with $a_1' > a_2'$

In this condition, it can be deduced from Equations (3)–(5) as

$$\gamma'_{D_2,x_1} = \frac{a_1' P|h_{SD_2} + \mathbf{h}_{RD_2}^H \boldsymbol{\Theta}_2 \mathbf{h}_{\mathrm{SR}}|^2}{a_2' P|h_{SD_2} + \mathbf{h}_{RD_2}^H \boldsymbol{\Theta}_2 \mathbf{h}_{\mathrm{SR}}|^2 + \sigma^2}, \tag{16}$$

$$\gamma'_{D_2,x_2} = \frac{a_2' P|h_{SD_2} + \mathbf{h}_{RD_2}^H \boldsymbol{\Theta}_2 \mathbf{h}_{SR}|^2}{\sigma^2}, \tag{17}$$

$$\gamma'_{E,x_2} = \frac{a_2' P|h_{SE}|^2|}{\sigma^2}, \tag{18}$$

$$\gamma'_{E,x_1} = \frac{a_1' P|h_{SE}|^2}{a_2' P|h_{SE}|^2 + \sigma^2}, \tag{19}$$

$$\gamma'_{D_1,x_1} = \frac{a_1' P|h_{SD_1} + \mathbf{h}_{RD_1}^H \boldsymbol{\Theta}_1 \mathbf{h}_{SR}|^2}{a_2' P|h_{SD_1} + \mathbf{h}_{RD_1}^H \boldsymbol{\Theta}_1 \mathbf{h}_{SR}|^2 + \sigma^2}, \tag{20}$$

so it can be further calculated $\gamma'_{D_1,x_1} > \gamma'_{D_2,x_1}$, and $min(\gamma'_{D_1,x_1}, \gamma'_{D_2,x_1}) = \gamma'_{D_2,x_1}$. Therefore, the secrecy rate of data x_1 and x_2 can be expressed as

$$R'_{Sx_1} = R'_{x_1} - R'_{Ex_1} = [\log_2(1+\gamma'_{D_2,x_1}) - \log_2(1+\gamma'_{E,x_1})]^+, \tag{21}$$

$$R'_{Sx_2} = R'_{x_2} - R'_{Ex_2} = [\log_2(1+\gamma'_{D_2,x_2}) - \log_2(1+\gamma'_{E,x_2})]^+, \tag{22}$$

where $[x]^+ = max(0, x)$; then, the secrecy rate can be obtained as

$$R'_S = R'_{Sx_1} + R'_{Sx_2}. \tag{23}$$

Considering the simple calculation, the Equations (19) and (20) can be directly substituted into Equation (23) as

$$\begin{aligned} R'_s &= \log_2\left(\frac{1+\gamma'_{D_2,x_1}}{1+\gamma'_{E,x_1}}\right)+\log_2\left(\frac{1+\gamma'_{D_2,x_2}}{1+\gamma'_{E,x_2}}\right) \\ &= \log_2\left[\frac{\left(1+\gamma'_{D_2,x_1}\right)\left(1+\gamma'_{D_2,x_2}\right)}{\left(1+\gamma'_{E,x_1}\right)\left(1+\gamma'_{E,x_2}\right)}\right]. \end{aligned} \tag{24}$$

3. Performance Analysis

In this section, because the location of the RIS is not fixed, the channel quality of user D_1 and user D_2 will also change in the process of continuous movement, thus affecting the change in the secrecy rate. In a communication system assisted by RIS-NOMA, since the fairness of users should be guaranteed when transmitting data, the change in the RIS position will also affect the distribution of the channel power by NOMA, so the secrecy rate of the channel is a topic worthy of further discussion. This problem can be solved by simply considering the change in the channel secrecy rate when different power allocation factors are used.

3.1. Ideal Phase Case

It is assumed that the phase shift is optimal, Specifically, $\left|h_{SU}+\mathbf{h}_{RU}^{H}\Theta\mathbf{h}_{SR}\right|^{2}, U \in \{D1, D2\}$ can be rewritten as

$$\begin{aligned}&\left|h_{SU}+\mathbf{h}_{RU}^{H}\boldsymbol{\Theta}\mathbf{h}_{SR}\right|^{2}\\&=|h_{SU}|^{2}+\left|\mathbf{h}_{RU}^{H}\boldsymbol{\Theta}\mathbf{h}_{SR}\right|^{2}+2\left|\mathbf{h}_{RU}^{H}\boldsymbol{\Theta}\mathbf{h}_{SR}\right||h_{SU}|\cos\left[\arg(h_{SU})-\arg\left(\mathbf{h}_{RU}^{H}\boldsymbol{\Theta}\mathbf{h}_{SR}\right)\right].\end{aligned} \tag{25}$$

From Equation (25), it can be verified that $\left|h_{SU}+\mathbf{h}_{RU}^{H}\boldsymbol{\Theta}\mathbf{h}_{SR}\right|^{2}$ is with an optimal result when $\cos\left[\arg(h_{SU})-\arg\left(\mathbf{h}_{RU}^{H}\boldsymbol{\Theta}\mathbf{h}_{SR}\right)\right]=1$, which implies that the phase shift for both the direct link between the source and destination, as well as the cascaded link is equivalent as $\arg(h_{SU})=\arg\left(\mathbf{h}_{RU}^{H}\boldsymbol{\Theta}\mathbf{h}_{SR}\right)$. Specifically, $\mathbf{h}_{RD_1}^{H}\boldsymbol{\Theta}_1\mathbf{h}_{SR}=\alpha\sum_{i=1}^{N}e^{j\phi_i}[\mathbf{h}_{SR}]_i[\mathbf{h}_{RD_1}]_i$ and $\mathbf{h}_{RD_2}^{H}\boldsymbol{\Theta}_2\mathbf{h}_{SR}=\alpha\sum_{i=1}^{N}e^{j\psi_i}[\mathbf{h}_{SR}]_i[\mathbf{h}_{RD_2}]_i$. Therefore, the optimal phase shift can be obtained

$$\begin{aligned}\phi_i&=\left[\arg(h_{SD_1})-\arg\left(\mathbf{h}_{RD_1}^{H}\boldsymbol{\Theta}\mathbf{h}_{SR}\right)\right],\\\psi_i&=\left[\arg(h_{SD_2})-\arg\left(\mathbf{h}_{RD_2}^{H}\boldsymbol{\Theta}\mathbf{h}_{SR}\right)\right].\end{aligned} \tag{26}$$

Combining the direct channel and the reflection channel, the sum channel gains from source to D_1 and D_2 can be simply expressed as

$$\begin{aligned}|h_{D_1}|^2&=\left[\sqrt{\beta_{SD_1}}+N\alpha\sqrt{\beta_{SRD_1}}\right]^2,\\|h_{D_2}|^2&=\left[\sqrt{\beta_{SD_2}}+N\alpha\sqrt{\beta_{SRD_2}}\right]^2,\end{aligned} \tag{27}$$

where $\beta_{SRD_1}=h_{SR}h_{RD_1}$, $\beta_{SRD_2}=h_{SR}h_{RD_2}$. From the previous chapter, it can be seen that if Equation (23) is directly substituted into Equation (22), it will be difficult to simplify and increase the complexity of calculation. Let $\rho=\frac{P}{\sigma^2}$ be the transmission SNR, because the proposed system works under the condition of high SNR by default; so, with the condition of $\rho \gg 1$, the approximation of $1+\rho \sim \rho$ can be used. Therefore, with $\gamma'_{D_2,x_1}=\frac{\rho a'_1|h'_{D_2}|^2}{1+\rho a'_2|h_{D_2}|^2}\approx \frac{a'_1}{a'_2}$, $\gamma'_{D_2x_2}=\rho a'_2|h'_{D_2}|^2$, $\gamma'_{D_1x_1}=\frac{\rho a'_1|h_{D_1}|^2}{1+\rho a'_2|h_{D_1}|^2}\approx\frac{a'_1}{a'_2}$, $\gamma'_{E,x_2}=\rho a'_2|h_{SE}|^2$, $\gamma'_{E,x_1}=\frac{\rho a'_1|h_{SE}|^2}{1+\rho a'_2|h_{SE}|^2}\approx \frac{a'_1}{a'_2}$, substitution into Equation (17) can give a simplified formula as

$$R'_s\approx\log_2[\frac{(1+\frac{a'_1}{a'_2})(1+\rho a'_2|h'_{D_2}|^2)}{(1+\frac{a'_1}{a'_2})(1+\rho a'_2|h_{SE}|^2)}]. \tag{28}$$

Since $\rho \gg 1$, we can further deduce $R'_s=\log_2[\frac{|h'_{D_2}|^2}{|h_{SE}|^2}]$. Similarly, when $a_1 < a_2$, we can obtain $R_S=\log_2[\frac{|h_{D_1}|^2}{|h_{SE}|^2}]$. It is clear that, for R'_s and R_s, x is constantly bigger than 0. Therefore, according to Jensen's inequality, for the concave function $log_2(x)$, an explicit closed-form expression for the upper bound of the channel capacity can be derived as

$$\mathbb{E}[\log_2(x)]\le\log_2(\mathbb{E}[x]). \tag{29}$$

3.2. Non-Ideal Phase Case

In practice, due to the hardware limitation, the RIS can not achieve ideal phase. Thus, for $a_1 < a_2$, we have

$$\begin{aligned}\gamma_{D_1,x_1} &= \frac{a_1 P|h_{SD_1} + \mathbf{h}_{RD_1}^H \mathbf{\Theta}_1 \mathbf{h}_{\mathrm{SR}}|^2}{\sigma^2} \\ &= \frac{a_1 P|h_{SD_1} + \sum_i^N [h_{RD_1}]_i |h_{SR}|_i e^{j\theta_i}|^2}{\sigma^2},\end{aligned} \tag{30}$$

$$\begin{aligned}\gamma_{D_1,x_1} &= a_1\rho|h_{SD_1} + \mathbf{h}_{RD_1}^H \mathbf{\Theta}_1 \mathbf{h}_{\mathrm{SR}}|^2 \\ &= a_1\rho\big||h_{SD_1}| + \sum_{i=1}^{N}|[h_{SR}]_i|\big|[h_{RD_1}]_i e^{\hat{j}_i}\big|^2 \\ &= a_1\rho\big||h_{SD_1}| + \sum_{i=1}^{N}|[h_{SR}]_i|\big|[h_{RD_1}]_i|\cos(\Theta_i) + j\sum_{i=1}^{N}|[h_{SR}]_i|\big|[h_{RD_1}]_i|\sin(\Theta_i)\big|^2 \\ &= a_1\rho\Big|\underbrace{|h_{SD_1}|^2 + \sum_{i=1}^{N}|[h_{SR}]_i|^2\big|[h_{RD_1}]_i\big|^2}_{A} + \underbrace{2|h_{SD_1}|\sum_{i=1}^{N}|[h_{SR}]_i|\big|[h_{RD_1}]_i|\cos(\Theta_i)}_{B} \\ &+ \underbrace{2\sum_{i=1}^{N-1}\sum_{k=i+1}^{N}|[h_{SR}]_i|\big|[h_{RD_1}]_i\big||[h_{SR}]_k|\big|[h_{RD_1}]_k\big|\big(\cos(\Theta_i)\cos(\Theta_k) + \sin(\Theta_i)\sin(\Theta_k)\big)\big|}_{C}.\end{aligned} \tag{31}$$

The corresponding capacity is given by $C_{D_1,x_1} = log_2(1+\gamma_{D_1,x_1})$ by which we attempt to obtain the ergodic capacity; so, $C_{D_1,x_1} = \mathrm{E} = C_{D_1,x_1}$; it is obvious that $|\beta_{SD_i}|$ following the exponential distribution with parameters $d_{SD_1}^{-\alpha}, d_{SR}^{-\alpha}, d_{RD_1}^{-\alpha}$ and $d_{SE}^{-\alpha}$. Where the $|\beta_i| = |h_i|^2$, and $|h_i|$ obey Rayleigh fading with parameters $\frac{1}{\sqrt{2}} d_i^{-\frac{\alpha}{2}}$, for i = SD_1, SR, RD_1, SE. The secrecy rate of D_1 in $case_1$ can thus be obtained from

$$R_s \approx \log_2(1 + \mathbb{E}(A) + \mathbb{E}(B) + \mathbb{E}(C)) - \log_2(1 + \mathbb{E}(\gamma_E)). \tag{32}$$

4. RIS Deployment Analysis

In this section, we analyze the influence of the RIS-NOMA-assisted IoV system with uncertain RIS deployment. Assuming that the channel gain is G_j, $j \in \{S, R, D_1, D_2\}$ and the path loss is $\alpha_k, k \in (1,2)$, leading to $\beta_{SD_1} = G_S G_{D_1} \alpha_1 d_{SD_1}$. In the same way, we have $\beta_{SD_2} = G_S G_{D_2} \alpha_2 d_{SD_2}$, $\beta_{SRD_1} = G_S G_R^2 G_{D_1} \alpha_1 d_{SR} d_{RD_1} d_{SD_1}$, $\beta'_{SRD_2} = G_S G_R^2 G_{D_2} \alpha_2 d_{SR} d'_{RD_2} d_{SD_2}$. By substituting the above results back into Equation (27), we have

$$N^2 G_R^2 d_{SR} d_{RD_1} + d_{SD_1} = N^2 G_R^2 d_{SR} d'_{RD_2} + d_{SD_2}. \tag{33}$$

Since the deployment position of the RIS and the distance from the RIS to S are variable, by means of the Cosine Theorem, the distance from RIS to user D_1 can be expressed as

$$d_{RD_1} = \sqrt{d_{SR}^2 + d_{SD_1}^2 - 2 d_{SR} d_{SD_1} \cos\theta}, \tag{34}$$

as well as the distance from the RIS to user D_2 is

$$d_{RD_2} = \sqrt{d_{SR}^2 + d_{SD_2}^2 + 2 d_{SR} d_{SD_2} \cos\theta}. \tag{35}$$

Clearly, if direct membership makes the formula very complicated, where d_{SR} and $cos\theta$ are variables, Taylor expansion can be adopted to solve such a problem, and the binary Taylor formula is

$$\begin{aligned} f(x_0+\Delta x, y_0+\Delta y) =& f(x_0,y_0)+\left(\Delta x\frac{\partial}{\partial x}+\Delta y\frac{\partial}{\partial y}\right)f(x_0,y_0)+\frac{1}{2!}\left(\Delta x\frac{\partial}{\partial x}+\Delta y\frac{\partial}{\partial y}\right)^2 \\ & f(x_0,y_0)+\cdots+\frac{1}{n!}\left(\Delta x\frac{\partial}{\partial x}+\Delta y\frac{\partial}{\partial y}\right)^n f(x_0,y_0)+R_n, \end{aligned} \tag{36}$$

where $R_n = o\left[\left(\sqrt{(\Delta x)^2+(\Delta y)^2}\right)^n\right]$. Letting d_{SR} and $cos\theta$ be x and y, respectively, we can obtain the following:

Let $x_0 = d_{SD_1}$ and $y_0 = 0$, which can be obtained after substitution in the formula and simplification as

$$\begin{aligned} d_{RD_1} =& (x^2+d_{SD_1}^2-2d_{SD_1}xy)^{\frac{1}{2}} \\ =& (x_0^2+d_{SD_1}^2-2d_{SD_1}x_0y_0)^{\frac{1}{2}}+\frac{1}{2}(x_0^2+d_{SD_1}^2-2d_{SD_1}x_0y_0)^{-\frac{1}{2}} \\ & (2x_0-2d_{SD_1}y_0)(x-x_0)+\frac{1}{2}(x_0^2+d_{SD_1}^2-2d_{SD_1}x_0y_0)^{-\frac{1}{2}} \\ & (-2d_{SD_1}x_0)(y-y_0)+o[(x-x_0)^2+(y-y_0)^2] \\ =& \frac{1}{\sqrt{2}}d_{SD_1}+\frac{1}{\sqrt{2}}d_{SR}-\frac{1}{\sqrt{2}}d_{SD_1}\cos\theta. \end{aligned} \tag{37}$$

Let $x_0 = d_{SD_2}$ and $y_0 = 0$, which can be obtained after substitution in the formula and simplification as

$$\begin{aligned} d_{RD_2} =& (x^2+d_{SD_2}^2+2d_{SD_2}xy)^{\frac{1}{2}} \\ =& (x_0^2+d_{SD_2}^2+2d_{SD_2}x_0y_0)^{\frac{1}{2}}+\frac{1}{2}(x_0^2+d_{SD_2}^2+2d_{SD_2}x_0y_0)^{-\frac{1}{2}} \\ & (2x_0+2d_{SD_2}y_0)(x-x_0)+\frac{1}{2}(x_0^2+d_{SD_2}^2+2d_{SD_2}x_0y_0)^{-\frac{1}{2}} \\ & (2d_{SD_2}x_0)(y-y_0)+o[(x-x_0)^2+(y-y_0)^2] \\ =& \frac{1}{\sqrt{2}}d_{SD_2}+\frac{1}{\sqrt{2}}d_{SR}-\frac{1}{\sqrt{2}}d_{SD_2}\cos\theta. \end{aligned} \tag{38}$$

Substituting the function values of d_{RD_1} and d_{RD_2}, we can obtain

$$\cos\theta = \frac{\sqrt{2}(d_{SD_1}-d_{SD_2})}{N^2G_R^2d_{SR}(d_{SD_1}+d_{SD_2})}+\frac{d_{SD_1}-d_{SD_2}}{d_{SD_1}+d_{SD_2}}. \tag{39}$$

5. Numerical Results

In this section, the performance of the proposed system is evaluated by numerical results. Assuming that all channels follow Rayleigh fading, the path loss index is set to 2.2. For simplicity, the position of each node is set to $(x_S, y_S) = (0,0), (x_{D_1}, y_{D_1}) = (80,0), (x_{D_2}, y_{D_2}) = (100,0)$.

Figure 2 shows the relationship between the total safe-rate of data transmission and the angle of the RIS position relative to the transmitter. In the proposed scheme, the transmission power is $P = 1$ dBm, and the number of reflective elements is fixed at 1000. As can be seen from the display results in Figure 2, when $a_1 < a_2$, the safe-rate gradually decreases with increase in the distance between the RIS and D_1. While $a_1 > a_2$, the security rate gradually increases with decrease in the distance between RIS and D_2. In addition, one can observe that there is an intersection between the security rates of data transmission, in which $\theta = 141^\circ$. This means that when the location of the RIS is deployed at this angle,

the secrecy sum-rates with different power factor allocation mechanisms are equal. It is also the threshold of the safe-rate, and the security at this time is the most unreliable. When the angle is less than 141°, the data will be transmitted by the power distribution factor transmission mode of $a_1 < a_2$. When the angle is larger than 141°, the data will be transmitted in the transmission mode of $a_1 > a_2$.

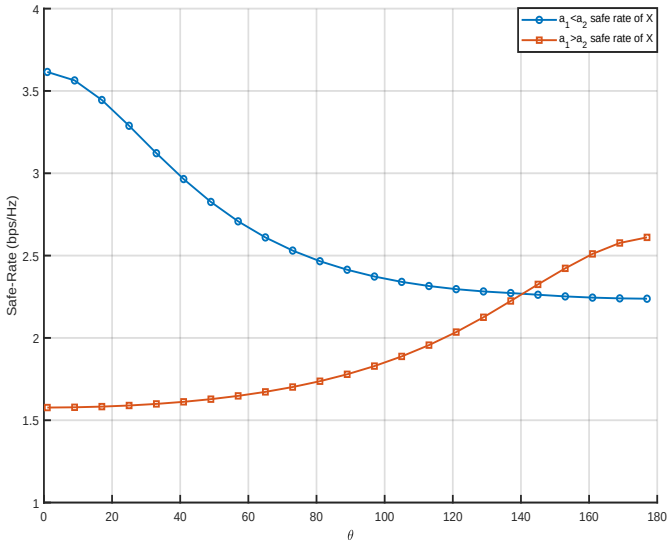

Figure 2. Total safe-rate versus location of the RIS.

Figure 3 shows the relationship between the safe-rate and the deployment position of the RIS. When the RIS is gradually further away from the user D_1, the transmission rate of data x_1 gradually decreases, while the eavesdropper directly eavesdrops on the data x_1 of S. The eavesdropping rate will not change due to the change in the deployment position of the RIS, but the change in the position of the RIS has little influence on the transmission rate of data x_2. In the proposed system, when $a_1 < a_2$, the eavesdropper first decodes signal x_2, and then decodes signal x_1. As we mentioned earlier in this work, the approximation of SNR for signal x_2 at the eavesdropper can be expressed as $\frac{a_2}{a_1}$, which means that the eavesdropping rate of signal x_2 is scarcely influenced by the RIS deployment location. Similar, the SNR for signal x_2 at D_2 is also scarcely influenced by the RIS deployment location, resulting in invariability of the safe rate of x_2. Furthermore, the safe-rate of the total data transmitted is similar to that of the data x_1. Similarly, when the RIS gradually approaches the user D_2, its channel quality gradually passes the user D_1, thus changing the power factor distribution of the channel. As a result, the safe-rate gradually increases after crossing the point. In this paper, the simulation assumes that the initial states are all on the same level with users D_1, D_2, and S.

Figure 4 shows that when the location of S is fixed and the distance between RIS and S is changed, the performance of the safe-rate is different. Assuming that the distances from S to RIS are 20 m, 30 m, and 40 m, respectively, one can observe that the safe-rate gradually increases as the deployment position of the RIS is closer to the S. This is because when the deployment position of the RIS is close to the S, the path loss decreases and the channel quality of the cascaded channel is improved, with the result that the safe-rate increases with decrease in the distance from the S. The changing trend of the curve in the figure is that the RIS gradually moves away from the user D_1, which weakens the data transmission quality of the RIS service user D_1 channel. Thus, the safe-rate of data x_1 decreases with increase in the angle. Similarly, because the deployment position of RIS is gradually closer to user D_2, the safe-rate of data x_2 gradually increases with increase in the deployment angle of the RIS relative to the S.

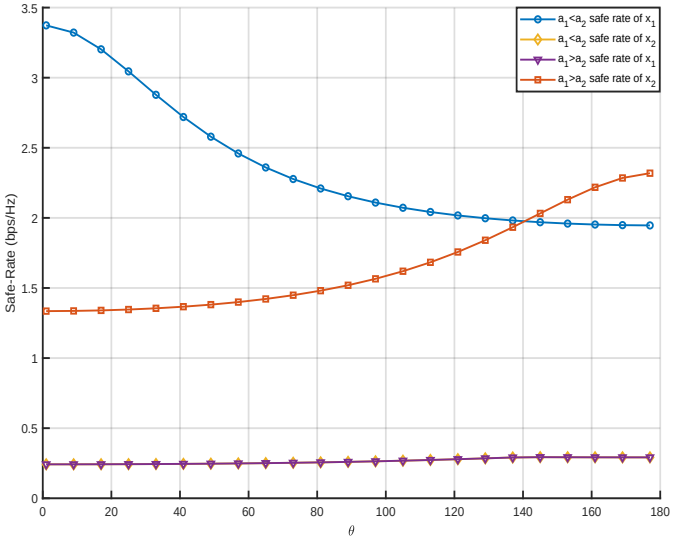

Figure 3. Safe-rates of x_1 and x_2 versus location of the RIS with different power allocations.

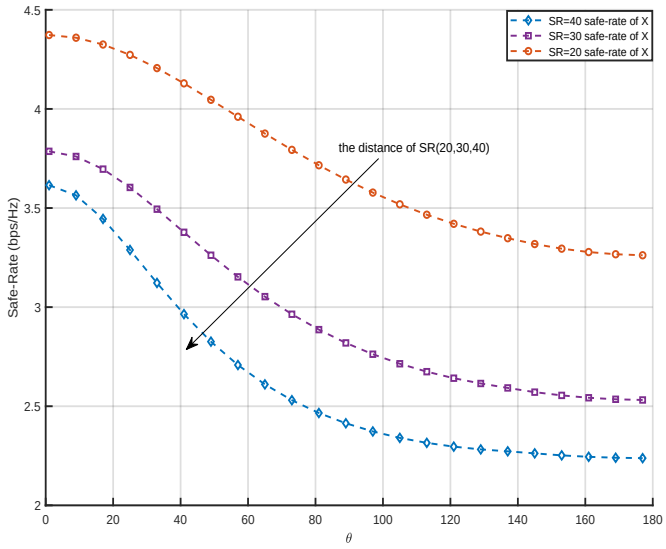

Figure 4. Safe-rate of x_1 versus the angle of the RIS relative to S in the case of different distances between the RIS and S.

Figure 5 shows the impact of increasing the number of RIS elements on the safe-rate of data x_1 when the location of S is fixed. Assuming that the number of elements of the RIS is 1000, 1500, and 2000, respectively, one can observe from the graphic information that the safe-rate is larger and larger with increase in the number of RIS reflection elements. Moreover, one can also see that the safe-rate gradually improves as the deployment position of the RIS gets closer to the S. This is because when the number of elements of the RIS increases, the channel quality of the cascade channel is enhanced, so the safe-rate will increase with increase in the RIS elements number. The changing trend of the curve in the figure is that the RIS gradually moves away from the user D_1, which weakens the data transmission quality of the RIS service user D_1 channel, so the safe-rate of data x_1 will decrease with increase in the angle. Similarly, because the deployment position of the RIS is gradually closer to user D_2, the safe-rate of data x_2 will gradually increase with increase in the deployment angle of the RIS relative to the S.

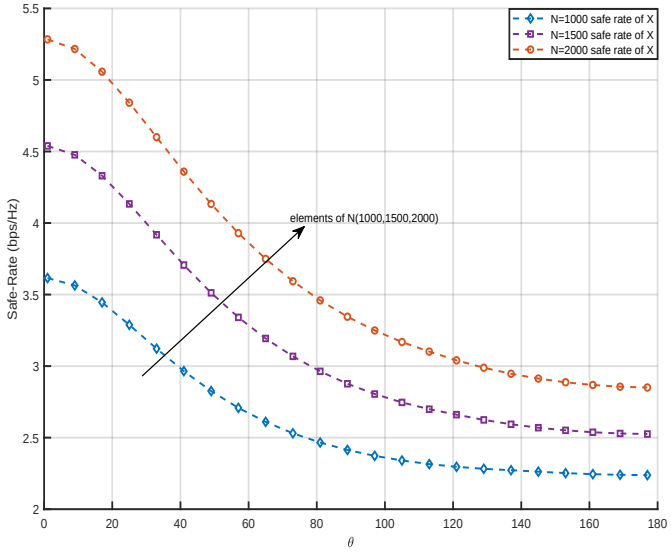

Figure 5. Relationship between the safe-rate of x_1 and location of the RIS under different numbers of RIS reflection elements.

Figure 6 plots the influence on the safe-rate of data x_1 when the location of S is fixed and the transmission power increases. Assuming that the transmission power is 1 dBm, -3 dBm, and -6 dBm, respectively, one can see that with increase in the transmission power, the safe-rate is larger and larger. This is because when the transmission power increases, the channel quality of the cascade channel is enhanced; thus, the safe-rate increases with increase in the transmission power. The changing trend of the curve in the figure is that the RIS gradually moves away from the user D_1, which weakens the data transmission quality of the RIS service user D_1 channel, so the safe-rate of data x_1 will decrease as the angle increases. Similarly, because the deployment position of the RIS is gradually closer to user D_2, the safe-rate of data x_2 will gradually increase with increase in the deployment angle of the RIS relative to the S.

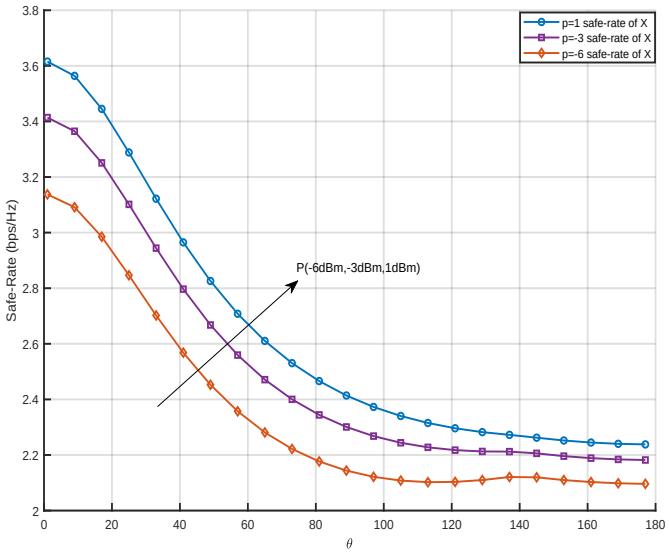

Figure 6. Relationship between safe-rate of data x_1 and transmission power.

Figure 7 draws the relationship between the power allocation factor coefficient and the angle of the RIS relative to the location of S. In the proposed scheme, the power is

set as $P = 1$ dBm and the number of RIS elements is assumed to be 1000; one can see from the display results in the figure that when the power allocation factor coefficient changes, it could not have a great influence on the trend of the simulation curve. When $a_1 < a_2$, the safe-rate of data transmission will gradually decrease with increase in the distance between the RIS deployment position and the user D_1. While $a_1 > a_2$, the safe-rate of data transmission will gradually increase with decrease in the distance between the deployment position of RIS and the user D_2. In the simulation, it can be found that even if the power allocation factor coefficient changes, the intersection point of the safe-rate of data transmission will not change, and the lowest value of the safe-rate will not change. Because there is no power allocation factor in Equation (36), the simulation results also verify the correctness of the formula derivation.

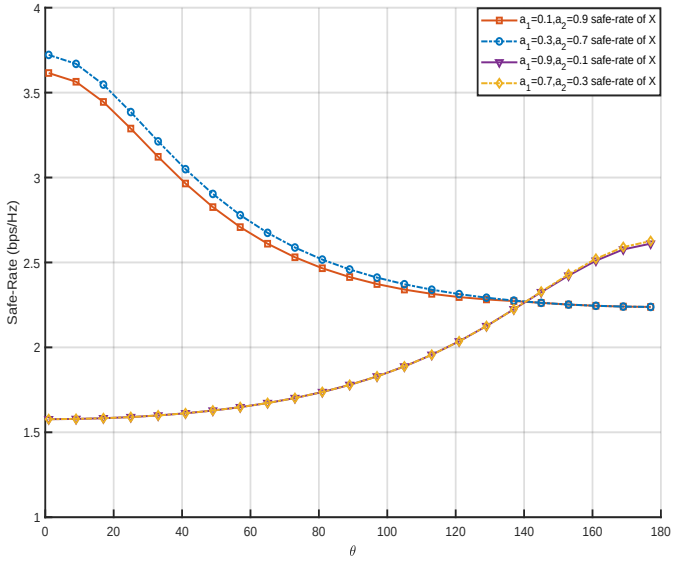

Figure 7. Relationship between safe-rate and power allocation factor.

6. Conclusions

This paper discussed the PLS of the RIS-NOMA system under the condition of uncertain RIS location, aiming to improve the safe-rate of data transmission under different channel conditions. In the proposed RIS-NOMA system, the RIS was designed to serve the user, while eavesdroppers tried to eavesdrop on the data of the source. It is worth noting that the deployment position of the RIS was not fixed, but changed within a certain range. In this paper, the equivalent safe-rate of two users was obtained through data analysis. In addition, this paper also deduced the minimum safe-rate required under different deployment angles of the RIS relative to the source. Numerical results obtained showed the deduced minimum safe-rate required with different angles of RIS relative to S, which verified the correctness of our analysis, as well as demonstrating the effectiveness of the proposed scheme. Apart from the analyzed results, the RIS-NOMA system is likely to offer further advantages, which could also be further refined in the future. The integration of RIS and NOMA, which could contribute effectively to power consumption and signal enhancement, is also a critical condition that requires further investigation.

Author Contributions: Software, Z.Z.; Validation, W.D.; Formal analysis, F.S.; Resources, H.Z.; Writing—original draft, J.G. All authors have read and agreed to the published version of the manuscript.

Funding: This work was funded in part by the Education Informatization Research Project in Jiangsu Province under Grant 2023JSETKT033, in part by the Qinglan Project in Jiangsu Province, and in part by Juxian Talent Project of Kangda College of Nanjing Medical University.

Data Availability Statement: The original contributions presented in the study are included in the article, further inquiries can be directed to the corresponding authors.

Conflicts of Interest: The authors declare no conflicts of interest.

References

1. Liu, L.; Feng, J.; Mu, X.; Pei, Q.; Lan, D.; Xiao, M. Asynchronous deep reinforcement learning for collaborative task computing and on-demand resource allocation in vehicular edge computing. *IEEE Trans. Intell. Transp. Syst.* **2023**, *24*, 15513–15526. [CrossRef]
2. Ni, Y.; Cai, L.; He, J.; Vinel, A.; Li, Y.; Mosavat-Jahromi, H.; Pan, J. Toward reliable and scalable internet of vehicles: Performance analysis and resource management. *Proc. IEEE* **2020**, *108*, 324–340. [CrossRef]
3. Zhang, J.; Letaief, K.B. Mobile edge intelligence and computing for the internet of vehicles. *Proc. IEEE* **2020**, *108*, 246–261. [CrossRef]
4. Li, H.; Ota, K.; Dong, M. Learning iov in 6g: Intelligent edge computing for internet of vehicles in 6g wireless communications. *IEEE Wirel. Commun.* **2023**, *30*, 96–101. [CrossRef]
5. Hazarika, B.; Singh, K.; Biswas, S.; Li, C.-P. Drl-based resource allocation for computation offloading in iov networks. *IEEE Trans. Ind. Inform.* **2022**, *18*, 8027–8038. [CrossRef]
6. Kazmi, S.A.; Ho, T.M.; Nguyen, T.T.; Fahim, M.; Khan, A.; Piran, M.J.; Baye, A.G. Computing on wheels: A deep reinforcement learning- based approach. *IEEE Trans. Intell. Transp. Syst.* **2022**, *23*, 22535–22548. [CrossRef]
7. Shi, J.; Du, J.; Shen, Y.; Wang, J.; Yuan, J.; Han, Z. Drl-based v2v computation offloading for blockchain- enabled vehicular networks. *IEEE Trans. Mob. Comput.* **2022**, *22*, 3882–3897. [CrossRef]
8. Wang, J.; Ke, H.; Liu, X.; Wang, H. Optimization for computational offloading in multi-access edge computing: A deep reinforcement learning scheme. *Comput. Netw.* **2022**, *204*, 108690. [CrossRef]
9. Chen, J.-X.; Yan, T.-Y.; Yang, J.-Y.; Ding, X.-H.; Yang, L.-L.; Li, Y. Dual-polarized heterogeneous stacked patch antenna with stable radiation performance and high efficiency. *IEEE Antennas Wirel. Propag. Lett.* **2024**, *23*, 2421–2425. [CrossRef]
10. Dai, L.; Jiao, R.; Adachi, F.; Poor, H.V.; Hanzo, L. Deep learning for wireless communications: An emerging interdisciplinary paradigm. *IEEE Wirel. Commun.* **2020**, *27*, 133–139. [CrossRef]
11. Yao, Z.; Cheng, W.; Zhang, W.; Zhang, H. Resource allocation for 5g-uav-based emergency wireless communications. *IEEE J. Sel. Areas Commun.* **2021**, *39*, 3395–3410. [CrossRef]
12. Zhang, Y.; Shen, K.; Ren, S.; Li, X.; Chen, X.; Luo, Z.Q. Configuring intelligent reflecting surface with performance guarantees: Op- timal beamforming. *IEEE J. Sel. Top. Signal Process.* **2022**, *16*, 967–979. [CrossRef]
13. Zhang, C.; Dong, M.; Ota, K. Heterogeneous mobile networking for lightweight uav assisted emergency communication. *IEEE Trans. Green Commun. Netw.* **2021**, *5*, 1345–1356. [CrossRef]
14. Wang, B.; Sun, Y.; Sun, Z.; Nguyen, L.D.; Duong, T.Q. Uavassisted emergency communications in social iot: A dynamic hypergraph coloring approach. *IEEE Internet Things J.* **2020**, *7*, 7663–7677. [CrossRef]
15. Lin, Y.; Wang, T.; Wang, S. Uav-assisted emergency communications: An extended multi-armed bandit perspective. *IEEE Commun. Lett.* **2019**, *23*, 938–941. [CrossRef]
16. Kafafy, M.; Ibrahim, A.S.; Ismall, M.H. Uplink Power Analysis of RIS-assisted Communication over Shared Radar Spectrum. In Proceedings of the 2022 5th International Conference on Communications, Signal Processing, and Their Applications (ICCSPA), Cairo, Egypt, 27–29 December 2022; pp. 1–5.
17. Xu, L.; Zhou, X.; Tao, Y.; Yu, X.; Yu, M.; Khan, F. AF Relaying Secrecy Performance Prediction for 6G Mobile Communication Networks in Industry 5.0. *IEEE Trans. Ind. Inform.* **2022**, *18*, 5485–5493. [CrossRef]
18. Andrawes, A.; Nordin, R.; Ismail, M. Energy harvesting with cooperative networks and adaptive transmission. In Proceedings of the 2017 IEEE Jordan Conference on Applied Electrical Engineering and Computing Technologies (AEECT), Aqaba, Jordan, 11–13 October 2017; pp. 1–6.
19. Chen, J.-X.; Yang, J.-Y.; Ding, X.-H.; Yan, T.-Y.; Li, Y.-L.; Yang, W.-W. A microwave/millimeter-wave shared-aperture fitering antenna with reused via structure. *IEEE Trans. Antennas Propag.* **2024**,*72*, 7377–7382. [CrossRef]
20. Gopala, P.K.; Lai, L.; El Gamal, H. On the Secrecy Capacity of Fading Channels. *IEEE Trans. Inform. Theory* **2008**, *54*, 4687–4698. [CrossRef]
21. Oh, M.K.; Lee, S.; Kang, Y.; Choi, D. Wireless Transceiver Aided Run-Time Secret Key Extraction for IoT Device Security. *IEEE Trans. Consum. Electron.* **2020**, *66*, 11–21. [CrossRef]
22. Sun, L.; Du, Q. Physical layer security with its applications in 5G networks: A review. *China Commun.* **2017**, *14*, 1–14. [CrossRef]
23. Ji, B.; Zhang, J.; Zhang, H.; Zhang, G.; Fan, H.; Mumtaz, S. Performance Analysis of RIS-Enhanced Secure Transmission for Symbiotic IoV Systems. *IEEE Trans. Cogn. Commun. Netw.* **2024**. [CrossRef]
24. Chen, L.; Zhu, J.; Yang, Y.; Boichenko, S. Physical Layer Security for RIS-V2V Networks With Different Eavesdropper Locations. *IEEE Internet Things J.* **2024**, *11*, 35791–35801. [CrossRef]
25. Wang, C.; Li, Z.; Xia, X.G.; Shi, J.; Si, J.; Zou, Y. Physical Layer Security Enhancement Using Artificial Noise in Cellular Vehicle-to-Everything (C-V2X) Networks. *IEEE Trans. Veh. Technol.* **2020**, *69*, 15253–15268. [CrossRef]

26. Liu, Y.; Su, Z.; Wang, Y. Artificial Noise-Assisted Beamforming and Power Allocation for Secure D2D-Enabled V2V Communications. In Proceedings of the 2021 IEEE 94th Vehicular Technology Conference (VTC2021-Fall), Norman, OK, USA, 27–30 September 2021; pp. 1–5.
27. Li, X.; Li, J.; Liu, Y.; Ding, Z.; Nallanathan, A. Residual Transceiver Hardware Impairments on Cooperative NOMA Networks. *IEEE Trans. Wirel. Commun.* **2020**, *19*, 680–695. [CrossRef]
28. Andrews, J.G. Interference cancellation for cellular systems: A contemporary overview. *IEEE Wirel. Commun.* **2005**, *12*, 19–29. [CrossRef]
29. Hou, T.; Liu, Y.; Song, Z.; Sun, X.; Chen, Y.; Hanzo, L. Reconfigurable Intelligent Surface Aided NOMA Networks. *IEEE J. Sel. Areas Commun.* **2020**, *38*, 2575–2588. [CrossRef]
30. Ding, Z.; Poor, H.V. A Simple Design of IRS-NOMA Transmission. *IEEE Commun. Lett.* **2020**, *24*, 1119–1123. [CrossRef]
31. Zhang, Y.; Zhang, G.; Chen, S.; Choi, J.; Ho, P.H. Optimal Element Allocation for RIS-Aided Physical Layer Security. *Wirel. Commun. Mob. Comput.* **2022**, *2022*, 4617366. [CrossRef]